Mathematical modelling and parametric study on a 30 kW_{el} high temperature PEM fuel cell based residential micro cogeneration plant

Behzad Najafi[*], *Alireza Haghighat Mamaghani*, *Andrea Baricci*, *Fabio Rinaldi*, *Andrea Casalegno*

Dipartimento di Energia, Politecnico di Milano, Via Lambruschini 4, 20156 Milano, Italy

Received 16 August 2014
Received in revised form
16 November 2014
Accepted 17 November 2014
Available online 13 December 2014

Introduction

Proton exchange membrane (PEM) fuel cells have been widely recognized as efficient and zero emission power sources suited for stationary power generation and mobile applica-tions. Amongst their numerous features, high power density, short start up due to low operating temperatures, high effi-ciency, long stack life, and noiseless operation make PEM fuel cells distinguished from the other types of fuel cells [1–5]. In addition, PEM fuel cells have a low thermal to electric ratio (TER) which provides them the superiority over combustion-based generation technologies for CHP applications at scales from 5 kW to 2 MW. Low temperature PEM (LT-PEM) fuel cells are the most common types of PEM fuel cells in which Nafion-based proton exchange membrane is employed and the operating temperature is around 80 °C. Several studies have been carried out so far on implementation of LT-PEM fuel cells for cogeneration and trigeneration purposes [6–9]. Ferguson et al. [10] developed a steady-state model of an LT-PEM fuel cell for building cogeneration applications and studied the effect of operating strategy and fuel cell sizing on the performance of the system. Radulescu et al. [11] performed an experimental and theoretical analysis on five identical CHP plants based on LT-PEM fuel cell installed in different cities in France. The employed system in their experiment could

* *Corresponding author*. Tel.: +39 02 2399 3840.
E-mail addresses: behzad.najafi@polimi.it (B. Najafi), alireza.haghighat@mail.polimi.it (A. Haghighat Mamaghani), andrea.baricci@polimi.it (A. Baricci), fabio.rinaldi@polimi.it (F. Rinaldi), andrea.casalegno@polimi.it (A. Casalegno).

Nomenclature

Acronyms

aux/proc	auxiliary to process flow rate ratio
CHP	combined heat and power
GDL	gas diffusion layer
HT-PEM	high temperature proton exchange membrane
LMTD	logarithmic mean temperature difference
LT-PEM	low temperature proton exchange membrane
MEA	membrane electrode assembly
OHM	ohmic
PBI	polybenzimidazole
PES	primary energy saving
PFSA	perfluorosulfonic acid
PrOX	preferential oxidation
RF	reforming factor
S/C	steam to carbon ratio
SMR	steam methane reforming
TER	thermal to electric ratio
WGS	water gas shift
WKO	water knock out

Symbols

E_{ID}	ideal voltage, V
E_a	activation energy, kJ mol^{-1}
f	friction factor
ΔH_{298K}	standard enthalpy of reaction, kJ $kmol^{-1}$
I	current, A
k	rate coefficient
K	equilibrium constant
LHV	low heating value, kJ kg^{-1}
$\dot{m}$	mass flow rate, kg s^{-1}
N	number of cells
Nu	Nusselt number
P_x	partial pressure of species x
P	power, kW
Pr	Prandtl number
$\dot{Q}$	the time rate of heat transfer, kW
r	rate of reaction, mol lit^{-1} s^{-1}
R	universal gas constant, kJ $kmol^{-1}$ K^{-1}
Re	Reynolds number
T	temperature, K
V	voltage, V

Subscripts

A	anode
C	cathode
cogen	cogeneration
el	electrical
th	thermal

Greek symbols

η_A	anodic voltage loss
η_C	cathodic voltage loss
η_{el}	electrical efficiency
η_I	first law efficiency
η_{th}	thermal efficiency
λ_{H_2}	anodic stoichiometric ratio

generate net electrical power of 5 kW and was equipped with a low temperature (e.g. around 60 °C) heat recovery system with 6 kW thermal output. Furthermore, Calise et al. [12] conducted a dynamic simulation of a polygeneration system based on solar collectors, absorption chiller and PEM fuel cells which is capable of providing electricity, space heating and cooling, and domestic hot water. In another study, steady state modelling and optimization of a small heat and power plant based on PEM fuel cell system was carried out [13]. In the optimization procedure conducted in this study, while keeping the power output constant, decreasing the natural gas consumption and increasing the heat recovery were considered as the objective functions.

Due to the importance of economic assessment in any newfound power generation system [14–17], some studies have taken into account the economic aspects of the PEM fuel cell based cogeneration systems. Contreras et al. [18] performed an energetic and economic study on the utilization of PEMFC based cogeneration systems in rural sector of Venezuela. Moreover, from the represented sensitivity analysis of electricity cost with time, a steady decrement of unit cost of electricity through time can be evidently seen which predicted the cost of 1$/kWh for 2020. Guizzi et al. [19] investigated the economic and energetic performance of a cogeneration system based on a PEM fuel cell fed by pure hydrogen produced in a membrane steam reformer. Besides the electrical power, the generated heat in the fuel cell and reformer was utilized to supply the needs of an office building, which finally resulted in net electrical and thermal efficiencies of 41.93% and 64.16% respectively at rated conditions. Roses et al. [20] compared the different membrane reactor configurations applied to a 2 kW micro-generation system based on an LT-PEM fuel cell. They underlined the key role of hydrogen production step in electrical and 2nd law efficiencies of the CHP system. In this regard, the adoption of membrane reactor technology (i.e. fixed bed and fluidized bed) resulted in overall electrical and 2nd law efficiencies of about 43% and 48% respectively, in comparison to 34% and 38% with conventional fuel processor.

Perfluorosulfonic acid (PFSA) polymer membranes specifically Nafion are the most widely used electrolytes in LT-PEM fuel cells owing to their elevated thermal and chemical stability, high ionic conductivity and electrical insulation [21,22]. Nevertheless, LT-PEM fuel cells with PFSA polymer membranes still have some shortcomings such as the slow kinetics of oxygen reduction, high material cost of noble catalysts, water management issues, and intensive required cooling [23,24]. In addition, the presence of carbon monoxide (CO) in reformate gas obtained by conventional fuel reforming methods adversely affects the LT-PEM performance due to the poisoning characteristic of CO for platinum anode catalyst. Accordingly, significant efforts have been made in order to mitigate or even evade all aforementioned obstacles on the way of efficient performance of the PEM fuel cells [25,26].

One of the well-known solutions to overcome the former issues, concerning the LT-PEMs, is the operation of PEM fuel cell at temperatures higher than 100 °C (high temperature PEM (HT-PEM) fuel cell). At high temperatures, the adsorption of

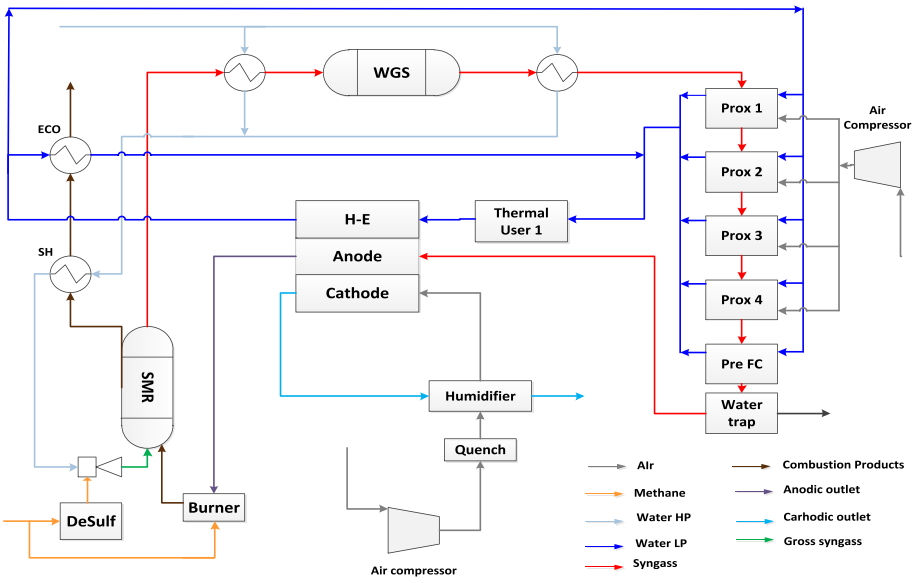

Fig. 1 – A schematic view of the LT-PEM Fuel cell based Plant's configuration.

CO onto the catalyst sites is much less considerable which not only improves the catalyst performance but also lessens the necessity for costly high hydrogen purity reformate gas. In addition, application of HT-PEM fuel cell leads to other advantages including simpler water management, due to the presence of single gaseous phase, easier stack cooling, and last but not least the possibility of cogeneration applications owing to the high temperature waste heat [27,28].

In order to operate at higher temperature, the employed polymeric membrane should be modified. Accordingly, an immense attention has been addressed to develop membrane materials with the capability of operation at higher temperatures [29,30]. Amongst various proposed membranes, polybenzimidazole (PBI) has been shown promise for high-temperature operation due to its high thermal stability. On the other hand, the problems of PBI membranes stemming from the low proton conductivity of pure PBI can be solved by doping the membrane by some acids (specifically the phosphoric acid) [31]. Accordingly, a few studies have been dedicated to investigation of the performance of HT-PEM fuel cell based systems. Arsalis et al. [32] proposed a micro CHP system based on an HT-PEM fuel cell stack with PBI membrane for providing the electric power (up to 1 kW_{el}), domestic hot water and space heating (up to 2 kW_{th}) for a single family household. They conducted a parametric study in order to investigate the effect of steam-to-carbon ratio, fuel cell operating temperature, combustor temperature and hydrogen stoichiometry on the overall performance of the system. The results demonstrated that the net system electrical, cogeneration thermal, and stack efficiencies are 27.62%, 55.46%, and 37.74% respectively, while the highest obtained combined cogeneration system efficiency was 83.08%. In another study, Arsalis et al. [33] applied a genetic algorithm based optimization strategy to the same HT-PEM fuel cell based micro-CHP system. Utilizing the optimization strategy, they could obtain a higher net electrical efficiency (objective function) of 41.2%, while the values of cogeneration thermal and total system efficiencies were found to be 49.7% and 91% respectively. Furthermore, Jannelli et al. [34] conducted a comprehensive study which enables one to compare the performance of cogeneration systems based on PEM fuel cells at three different temperature levels, 67 °C, 160 °C, and 180 °C, with different membranes. Their results revealed that the systems based on the HT-PEM fuel cells are characterized by high electrical efficiency of 40% and first law efficiency of 79%.

In the present study, a new system design for an existing low temperature PEM fuel cell based cogeneration plant (Sidera30) is proposed in which the conventional LT-PEM fuel cell stack has been replaced with an HT-PEM one. Considering the above mentioned advantages of the HT-PEM fuel cells, including higher CO tolerance and no water management issues, the fuel processor unit of the plant is simplified and the water management system is eliminated. The water circuits, which are employed for thermal management, are accordingly modified and two recuperators, in order to provide heat recovery for the anodic and cathodic flows, have been added.

In the next step, detailed mathematical models for the fuel processor components, PEM fuel cell stack, the heat exchangers, and all other auxiliary components of the plant have been developed. In order to model the fuel processor and the heat exchangers, the geometries and the kinetic characteristics of these components in the existing system have been employed. Exploiting the provided models, the electrical and thermal performance of the system have been determined and the obtained results have been compared with the performance indices achieved for the previous plant at design condition. Considering the fact that the physical models have been developed for all components of the plant, the model has the capability to estimate the behaviour of the plant in wide range of operating conditions. Accordingly in the last step, in order to investigate the behaviour of the system and to determine operating conditions of the system resulting in higher performances, a sensitivity analysis on the key parameters of the system has been conducted. Firstly, in order to

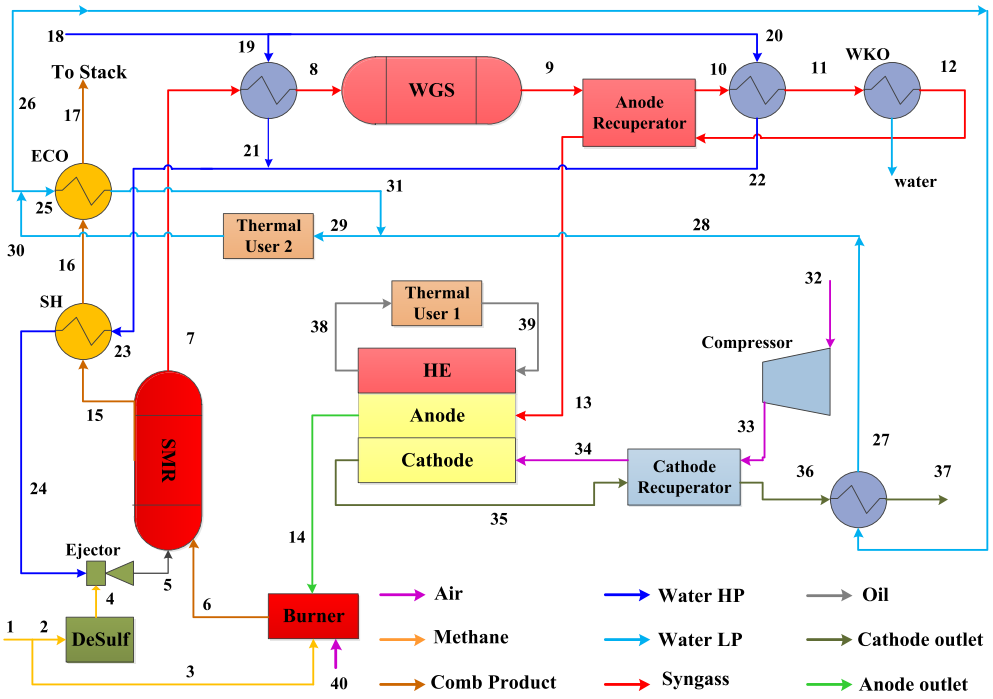

Fig. 2 – Configuration of the proposed HT-PEMFC based plant.

study the behaviour of the fuel processor, the effects of S/C and aux/proc ratios have been studied and consequently four operating points with the highest reforming factors and lowest CO concentrations have been chosen. In the next step, at each selected operating condition, the outcome of variations in stack design parameters including the operating temperature of the cell, current density, and the anodic stoichiometric ratio on the performance of the plant has been studied.

Plant description

Configuration of LT-PEM fuel cell based plant (Sidera30)

Sidera30 is a cogeneration plant based on a PEM fuel cell stack for residential applications which has been designed and produced by "ICI Caldaie S.p.A". A schematic view of the Sidera30 plant is demonstrated in Fig. 1. Natural gas, which is fed to the plant, is mixed with the high pressure steam inside the ejector and the mixture of higher pressure (than that of methane) is introduced into the steam reforming reactor in which it is partly converted into hydrogen and carbon monoxide. The generated syngas in the next step enters the pre water gas shift heat exchanger in which its temperature is decreased. The cooled syngas then enters the water gas shift reactor in which a part of the generated CO will be converted into more hydrogen and CO_2. Afterwards, the syngas is cooled down again in the post WGS heat exchanger to be in an acceptable temperature range required by the next reactor. The remained carbon monoxide is then reduced to an acceptable level in the PrOX units. In each PrOX reactor, a part of the remaining CO is burnt and the syngas enters the next reactor in which it is first cooled down and then undergoes a preferential oxidation reaction. The syngas which is leaving the last PrOX reactor will include approximately 5 ppm of CO. The produced syngas is cooled down again in the pre FC heat exchanger to reach the operating temperature of the stack. The pre FC heat exchanger is followed by a water trap in which most of the contained water, which is condensed, is retained. The syngas which has lost part of its containing water then enter the anodic side of the LT-PEM fuel cell. The anodic flow after undergoing the electrochemical reaction within the stack enters the burner in which the remaining hydrogen within the flow is burnt together with the added auxiliary methane.

In the other side, owing to the fact that the cathodic flow should also be humidified, the ambient air which is compressed by the cathodic compressor enters the quench where a specific amount of water is added to the air stream. The quenched air then enters the humidifier where the humidity and the heat contained in the cathode outlet are partly recovered. The warmed and humidified air is then introduced into the cathode.

The high pressure circuit is an open circuit in which the water is taken from a tank at 30 °C. It is also assumed that the water is pressurized by the HP pump to 8 bars. In this circuit, the water exiting the high pressure pump is divided into two flows going through the pre-WGS and post-WGS heat exchangers. Both flows are mixed in the next step and the mixture will subsequently enter the superheater in which the energy content, remaining in the flue gases, will be recovered to produce superheated steam which will be fed to the ejector in the next step.

The low pressure water is a closed circuit which supplies the thermal demand of the system. The water which is leaving

the stack heat exchanger is divided into the flows which pass through the PrOX heat exchangers, pre-FC heat exchanger and the economizer. These flows are then mixed and enter the thermal use where they can yield the heat which they have recovered.

Configuration of the proposed HT-PEM fuel cell based plant

In the proposed HT-PEMFC based system, owing to the previously stated advantages of HT-PEMFCs, including higher CO tolerance and the elimination of water management issues, the PrOX reactors and the cathodic air humidification system have been removed. Considering elevated temperature of the syngas leaving the WGS reactor and also the cathodic outlet, two recuperators have been utilized in order to warm up the streams entering the stack. Further, considering the higher temperature of the stack coolant, a separate thermal use circuit has been designed only for the stack. Based on the mentioned design modification, the operation principle of the plant, demonstrated in Fig. 2, can be explained as follows:

In the first step, the mixture of natural gas and superheated steam enters the steam reformer where it undergoes the steam methane reforming reaction producing hydrogen and CO. The generated syngas subsequently passes through the WGS reactor in which the shift reaction takes place and a fraction of the CO is converted into CO_2 and an acceptable molar fraction of CO remains in the syngas. The processed syngas afterwards enters the anodic side of the HT-PEM fuel cell where the hydrogen is consumed through the electro-chemical reaction generating electricity. The anodic outlet, which still includes unconsumed amounts of hydrogen and methane, is directed to the burner to burn together with the auxiliary methane generating combustion products which will provide the required energy of the SMR reactor and subsequently produce the steam and warm water in the superheater and economizer respectively. In the other side, the compressed air is fed to the cathodic side providing the required oxygen. Two recuperators are also employed for warming up the fuel cell inlet streams. Prior to the anodic recuperator, a water knock out (WKO) has been utilized to considerably decrease the water content of anodic inlet stream. A heat exchanger preceding the anodic recuperator is also employed to recover the remained heat in the syngas for producing high pressure saturated water.

Model description

Fuel processor

Steam methane reformer reactor (SMR)
Steam reforming of methane is still the predominant method for hydrogen production and fulfils about 50% of hydrogen demand worldwide [35]. The model takes into account a 1D steady state and non-isothermal plug flow reactor with shell and tube heat exchanger design. The composition of the catalyst and support, due to the confidentiality of the manufacturer's data cannot be stated. The model considers two separate working media; the tube side filled with catalysts, in which the reactions take place, and the shell side where the hot gases from the burner pass and provide the required energy for extremely endothermic reforming reactions. The dimensions of the modelled SMR reactor are obtained from the fuel processor of the existing LT-PEM plant and the developed model is consequently validated using the experimental data obtained from the mentioned plant.

The three main reactions taking place in a steam reforming process are as follows:

$$CH_4 + H_2O \Leftrightarrow CO + 3H_2 \quad \Delta H_{298K} = +206\ \text{kJ/mol} \tag{1}$$

$$CO + H_2O \Leftrightarrow CO_2 + H_2 \quad \Delta H_{298K} = -41\ \text{kJ/mol} \tag{2}$$

$$CH_4 + 2H_2O \Leftrightarrow CO_2 + 4H_2 \quad \Delta H_{298K} = -165\ \text{kJ/mol} \tag{3}$$

The exothermic water gas shift reaction is fast enough to be considered in equilibrium. The steam reforming reaction is strongly endothermic and is favoured at low pressure and high temperature. Xu and Froment [36] have developed a general and realistic Langmuir–Hinshelwood type kinetic model for the steam reforming of methane considering the water–gas shift reaction to occur in parallel with the steam reforming reactions. The kinetics equations are:

$$r_1 = \frac{k_1}{P_{H_2}^{2.5}} \frac{P_{CH_4}P_{H_2} - P_{H_2}^3 P_{CO}/K_1}{DEN^2} \tag{4}$$

$$r_2 = \frac{k_2}{P_{H_2}} \frac{P_{CO}P_{H_2O} - P_{H_2}P_{CO_2}/K_2}{DEN^2} \tag{5}$$

$$r_3 = \frac{k_3}{P_{H_2}^{3.5}} \frac{P_{CH_4}P_{H_2O}^2 - P_{H_2}^4 P_{CO_2}/K_3}{DEN^2} \tag{6}$$

$$DEN = 1 + K_{CO}P_{CO} + K_{H_2}P_{H_2} + K_{CH_4}P_{CH_4} + \frac{K_{H_2O}P_{H_2O}}{P_{H_2}} \tag{7}$$

$$k_i = A(k_i)\cdot\exp[-E_i/(RT)], \quad \text{for } i = 1,\ldots,3 \tag{8}$$

$$K_i = A(K_i)\cdot\exp[-\Delta H_i/(RT)], \quad \text{for } i = 1,\ldots,3 \tag{9}$$

$$K_j = A(K_j)\cdot\exp[-\Delta H_j/(RT)], \quad \text{for } j = CH_4,\ H_2O,\ CO,\ H_2 \tag{10}$$

The kinetic coefficients employed in the preceding equations are extracted from Ref. [36].

Water gas shift reactor
To enhance the hydrogen yield besides removing the carbon monoxide, which is detrimental to the stack, the water gas shift (WGS) reaction is carried out on the SMR outlet syngas:

$$CO + H_2O \Leftrightarrow CO_2 + H_2 \quad \Delta H_{298K} = -41\text{kJ/mol} \tag{11}$$

The heat exchanger placed prior to the WGS reactor decreases the temperature of the inlet stream to WGS reactor to a desired level. The thermodynamic equilibrium constant of the WGS reaction can be expressed as [37]:

$$K_p = e^{\left(\frac{4400}{T} - 4.036\right)} \tag{12}$$

For the shift converter, the kinetics equation according to Keiksi et al. [38] for high temperature WGS is:

$$r_{WGS} = k_0 \cdot \exp\left(\frac{-E_a}{RT}\right)(1-\beta)P_{CO}^{1.1}P_{H_2O}^{0.53} \quad (13)$$

where $E_\alpha = 95000$ kJ/mol is the activation energy, $R = 8.314$ J/(K mol), ln (k_0) = 26.1 is pre-exponential factor, and β is the reversibility factor defined as:

$$\beta = \frac{1}{K_P}\frac{P_{CO_2}P_{H_2}}{P_{CO}P_{H_2O}} \quad (14)$$

HT-PEMFC stack

The HT-PEM fuel cell stack consists of three main parts including the membrane electrode assembly (MEA),the pre-heater and the oil cooling circuit. In the pre-heater, the reactants (the syngas and the compressed air) exchange heat with the circulating oil to reach the stack inlet temperature. In the membrane electrode assembly, hydrogen and oxygen are converted into water while generating electrical power. The MEA is made up of several layers including: the cathodic and anodic channels (where the air and the syngas flow), the cathodic and anodic gas diffusion layers (GDL), which provide a pathway for the reactants from the channels to the catalyst layer, and finally the cathodic and anodic electrodes where the electrochemical reaction occurs. Through the electrolyte membrane (in this study PBI), which separates the electrodes, the protons are transported from the anode to the cathode. The air and the syngas are supposed to flow in co-current configuration as is generally done in real systems to reduce the pressure difference across the MEA. Two hypotheses have been assumed: negligible pressure drop along the channels and the fact that the reactants are divided equally in the channels. Assuming the preceding hypotheses provides the possibility to model a single channel and extend the corresponding results to the whole stack. The considered stack geometric parameters are reported in Table 1.

The MEA domain is modelled employing a quasi 2D approach: the channel is considered monodimensional in the flow direction and monodimensional through the MEA direction. Within the channel, the hydrogen and oxygen are gradually consumed owing to the electrochemical reactions while water is consequently produced. Furthermore, the mass conservation is employed in order to calculate the profiles of the species concentration, in particular hydrogen, oxygen, water and carbon monoxide, along the channels.

The reaction rate (the current density) is determined locally by solving the following identity which associates the cell voltage to the ideal voltage:

$$V = E_{ID} - \eta_{OHM} - \eta_C - \eta_A \quad (15)$$

$$P_{stack} = V_{cell} I_{stack} N \quad (16)$$

Table 1 – The geometric parameters of the HT-PEM fuel cell based stack.

Geometric parameter	Value
Channel length (cm)	76.25
Channel heigh (cm)	0.2
Cell width (cm)	7.6
Number of channels	38
Number of cells	440

where E_{ID} is the ideal voltage determined using Nernst equation, V is the single cell voltage, η_{OHM} is the ohmic loss, and η_C and η_A are the cathodic and anodic activation losses respectively. The ideal voltage is calculated, as a function of temperature, from the Gibbs free energy formation data. The Ohmic loss is supposed to follow Ohm's law and is the sum of the resistances of the GDLs, bipolar plate, and the electrolyte. It is assumed that the electrolyte conductivity follows Arrhenius law and it is taken from Ref. [39].

Mass transport within the GDL is modelled considering multi component gas diffusion using Stefan–Maxwell phenomenological law [40]. The binary diffusion coefficients are determined employing the correlation proposed by Fuller et al. [41] and afterwards are corrected to take into account the porous media porosity and tortuosity.

The cathodic electrode is considered to be homogeneous and its corresponding activation losses are supposed to follow the Tafel Law, first order with respect to oxygen concentration [42]:

$$\eta_C \equiv b \cdot \log\left(\frac{i}{i_*}\right) + b \cdot \log\left(\frac{C_{ref}}{C_{O_2,el}}\right) \quad (17)$$

where i_* is the reference exchange current density which follows an Arrhenius like behaviour and b which is determined using the following relation, is the Tafel slope:

$$b = RT/(\alpha_C F) \quad (18)$$

In order to enhance the accuracy of the proposed model, the poisoning effect, owing to the presence of carbon monoxide, on the anodic catalyst is taken into account in the anodic activation losses. The hydrogen and CO oxidation currents are calculated employing the Butler–Volmer equation [26]:

$$i_{H_2} \equiv i_{*,H_2} \cdot \vartheta_H \cdot 2\sinh\left(\frac{\eta_A}{b_A}\right) \quad (19)$$

$$i_{CO} \equiv i_{*,CO} \cdot \vartheta_{CO} \cdot 2\sinh\left(\frac{\eta_A}{b_A}\right) \quad (20)$$

$$i = i_{CO} + i_{H_2} \quad (21)$$

where, by definition, the sum of the coverage of all the species must be equal to 1:

$$\vartheta_{FREE} = 1 - \vartheta_H - \vartheta_{CO} - \vartheta_{H_2PO_4^-} \quad (22)$$

The coverage of phosphoric acid ($\vartheta_{H_2PO_4^-}$) is taken from Refs. [43], while the coverage of hydrogen and CO (ϑ_H and ϑ_{CO}) are computed considering the equilibrium of adsorption using Langmuir adsorption for hydrogen and Frumkin adsorption for carbon monoxide.

In HT-PEM, the transport of proton through the membrane is assisted by phosphoric acid and occurs even in high dehydration conditions (RH <5%). The predominant mechanism is of Grotthus type, which is based on the amphoteric characteristics of phosphoric acid that is able to transport the protons by forming a chain which acts as an electrolyte. Water is the only species which passes through the electrolyte and the transport of water through the membrane has a diffusive character and can be represented by Fick's law, assuming

Table 2 – The values of the parameters used for the HT-PEM fuel cell modelling.

Symbol	Value	Description
C_{ref}/mol cm^{-3}	$5.88\cdot10^{-6}$	Reference O_2 concentration
δ_{GDL}/cm	0.04	GDL thickness, anode/cathode
δ_{MEM}/cm	0.015	Membrane thickness [43]
ε/τ_{GDL}/-	0.084	Porosity/tortuosity GDL, anode/cathode
$\theta_{H_2PO_4^-}$/-	0.05	$H_2PO_4^-$ coverage [43]
E_0/V	$1.256-2.4\cdot10^{-4}$ T	Ideal potential
α_C/-	0.85	Charge transfer coefficient cathode [39]
E_{ORR}/J mol^{-1}	$102.86\cdot10^3$	Activation energy ORR [43]
$i_{0,ORR}$/A cm^{-2}	$3.28\cdot10^{-6}$	Exchange current density ORR [43]
α_A/-	0.5	Charge transfer coefficient anode [43]
E_{HOR}/J mol^{-1}	$2.5\cdot10^3$	Activation energy HOR
$i_{0,HOR}$/A cm^{-2}	$1.25\cdot10^3$	Exchange current density HOR [26]
$E_{COR,\ C}$/J mol^{-1}	$127\cdot10^3$	Activation energy COR [26]
$i_{0,COR}$/A cm^{-2}	$2.2\cdot10^{13}$	Exchange current density cathode [26]
$E_{ADS,H}$/J mol^{-1}	$10.4\cdot10^3$	Activation energy hydrogen adsorption [26]
$k_{ADS,H}$/cm s^{-1}	5.96	Hydrogen adsorption constant [26]
$E_{ADS,CO}$/J mol^{-1}	$47.3\cdot10^3$	Activation energy CO adsorption [26]
$k_{ADS,CO}$/cm s^{-1}	$1.5\cdot10^5$	CO adsorption constant [43]
$E_{DES,H}$/J mol^{-1}	$98.3\cdot10^3$	Activation energy hydrogen desorption [26]
$k_{DES,H}$/cm s^{-1}	$2.5\cdot10^3$	Hydrogen desorption constant [26]
$E_{DES,CO}$/J mol^{-1}	$147\cdot10^3$	Activation energy CO desorption [26]
$k_{DES,CO}$/cm s^{-1}	$1.03\cdot103$	CO desorption constant [26]
β_{CO}/-	0.1	Frumkin isotherm symmetry factor [26]
r_{CO}/J mol^{-1} K^{-1}	56.5	Frumkin isotherm lateral interaction parameter [26]
σ_{GDL}/S cm^{-1}	9	GDL conductivity [42]
Σ_0/S cm^{-1} K^{-1}	$9.4\cdot10^3$	Membrane conductivity parameter [39]
$E_{\sigma,MEM}$/J mol^{-1}	$18.5\cdot10^3$	Activation energy membrane conductivity [39]
D_m/cm^2 s^{-1}	0.001	Membrane water permeation coefficient

equilibrium of water in the vapour phase and in acid at the interface of the electrode.

It is noteworthy that in the previous experiments carried out by the co-authors [44] the effect of crossover was measured to be less than 1 mA/cm^2. Since this value is considerably smaller than the range of operating current densities considered in the present study (100–400 mA/cm^2), the cross over effect has not been taken into account in the HT-PEM model employed in the present work.

The values of the parameters, used for the HT-PEM fuel cell stack modelling in the present study work, are summarized in Table 2.

Auxiliary components

Ejector

As was previously explained, the high temperature steam, which has been produced in the superheater, and the process methane enter the ejector. For modelling the ejector the single phase thermodynamic model, proposed in Ref. [45] based on isobaric mixing, has been utilized in which the ejector structure is divided into four main sections of the nozzle, the suction chamber, the constant and the diffuser.

Heat exchangers

In order to model the heat exchangers, an iterative LMTD method has been employed. In order to calculate the global heat transfer coefficient, the internal and external convective heat transfer coefficients should be evaluated. The Churchill–Bernstein relation for cross flow heat exchange over tubes is used for determining the external convective heat transfer coefficient [46,47], while Gnielinski equation [46] is utilized for determining the internal heat transfer coefficient.

Results and discussion

Model validation

Fuel processor

As was previously stated, the geometries and kinetic characteristics of the steam methane reformer and the WGS reactors, employed in the present plant, are obtained from an existing LT-PEM fuel cell based cogeneration plant (Sidera30), designed by ICI Caldaie S.p.A, a prototype of which was previously installed in the Department of Energy of Politecnico di Milano. Accordingly, the model validation of the fuel processor has been carried out at the operating conditions of the mentioned system. The behaviour of the fuel processor has been investigated by measuring the syngas compositions at the outlet of the reformer and WGS units. The outlet syngas compositions have been determined employing a gas chromatograph (GC) with an acceptable accuracy. The obtained dry fractions at the WGS and SMR outlets have been compared with the experimental data in Table 3. The temperatures of the syngas at the outlet of the fuel processor reactors and the superheater and the corresponding values extracted from experimental data are given in Table 4. Even though there is a subtle difference between the experimental and obtained data, it can be observed that the presented model can predict the reformer's performance with a good agreement with the experimental data.

HT-PEM fuel cell stack

The polarization curves of the fuel cell obtained from the model and the experimental results given by Bergmann et al. [43], at different temperatures (130 °C –160 °C) and with pure hydrogen and CO concentration up to 1.6%, are compared in Fig. 3. As can be noted in this figure, an acceptable accordance between the obtained results and the experimental data can be vividly seen which verifies the validity of the developed model.

Performance indices

In this section the most relevant indicators of the performance of the CHP plant can be defined before further discussion on the obtained results. The net electrical efficiency ($\eta_{net,el}$), gross electrical efficiency ($\eta_{gross,el}$), thermal efficiency (η_{th}), the first law efficiency (η_I), and primary energy savings (PES) index have been employed to investigate the performance of the proposed micro-CHP system.

The net electrical efficiency is defined as the net electrical power output divided by the chemical energy input to the system. The net power output is the remaining power generated by the fuel cell stack after losses and subtracting auxiliaries. In addition, the gross electrical efficiency is defined as the ratio of power generated in the stack and the chemical energy input to the system.

$$\eta_{net,el} = \frac{\dot{P}_{el,net}}{\dot{m}_{CH_4,in} LHV_{CH_4}} \tag{23}$$

$$\eta_{gross,el} = \frac{\dot{P}_{el,gross}}{\dot{m}_{CH_4,in} LHV_{CH_4}} \tag{24}$$

The thermal efficiency is defined as the recovered useful heat ($\dot{Q}_{user}$) divided by the chemical energy input to the system. As a result, the first law efficiency of the plant is the sum of the net power output and the recovered useful heat divided by the chemical energy input to the system.

$$\eta_{th} = \frac{\dot{Q}_{user1} + \dot{Q}_{user2}}{\dot{m}_{CH_4,in} LHV_{CH_4}} \tag{25}$$

$$\eta_I = \frac{\dot{P}_{el,net} + \dot{Q}_{user1} + \dot{Q}_{user2}}{\dot{m}_{CH_4,in} LHV_{CH_4}} \tag{26}$$

And finally, the primary energy savings (PES) index is calculated according to the EU Directive on cogeneration:

$$PES = 1 - 1 \Big/ \left[\frac{\eta_{net,el}}{\eta_{el,cogen} \times p} + \frac{\eta_{th}}{\eta_{th,cogen}} \right] \tag{27}$$

Table 3 – Outlet dry molar fractions of the SMR and WGS reactors obtained from the model and the provided experimental data.

Dry molar fraction	CH_4	H_2	CO	CO_2	N_2
SMR outlet (Experimental)	0.0452	0.749	0.051	0.151	0.0047
SMR outlet (Model)	0.0528	0.745	0.0478	0.1504	0.00418
WGS outlet (Experimental)	0.045	0.753	0.012	0.1856	0.0044
WGS outlet (Model)	0.0508	0.754	0.00865	0.182	0.00403

Table 4 – Outlet temperatures of the fuel processor reactors and superheater obtained from the model and the provided experimental data.

Parameter	Model (°C)	Experimental (°C)
Syngas temperature at SMR outlet	577	590
Syngas temperature at WGS outlet	339	331
Steam temperature at superheater outlet	535	527

where the reference electrical and thermal efficiencies for the separate generation of electricity and heat are 52.5% and 90% respectively. It is assumed that 50% of electricity production of the plant is consumed onsite and 50% is injected to the local grid, therefore the intermediate grid efficiency coefficient, p, is equal to 0.8925 [48].

Base case analysis and performance comparison of two plants

The base case operating parameters of the HT-PEM based CHP plant and the corresponding values of the LT-PEM based system (Sidera30) are demonstrated in Table 5. It is worth mentioning that, due to the higher CO tolerance of the HT-PEMFC, the proposed system can operate at lower anodic stoichiometric ratio (i.e. 1.2) compared to the corresponding value of the existing LT-PEM based plant (i.e. 1.6).

Performance of the proposed system, in the base case condition, has been determined and a comparison between the performance indices obtained for the proposed system and the ones achieved for Sidera30 is given in Table 6. As can be observed in this table, considerably higher electrical efficiency has been obtained for the proposed plant, the advantage which is mainly due to the simplification of the water management system, leading to lower auxiliary losses and elimination of the PrOX reactors. Expectedly, since the obtained electrical efficiency for the proposed plant is significantly higher than the one of the LT-PEM based plant, the corresponding gained PES is also notably higher than the one of the previous plant. It should be pointed out that, in the present work, the natural gas is assumed to be composed of 98.6% of methane and 1.4% of nitrogen.

It should also be mentioned that, in the present study, the thermal and electrical production of the system are considered to be constant. In fact, the plant is designed to meet a specific portion of the building's thermal demand and the system is considered to be grid-connected. Nonetheless, it should be pointed out that, in case the system is designed to supply the whole demand of the building, the nature of thermal and electrical profiles will be a key factor in determining the performance indices of the plant.

Parametric study

In the second phase of the present study, in order to investigate the effect of different operating parameters on the performance of the system, a parametric study is carried out. Accordingly, in order to study the behaviour of the fuel processor, the mixed effect of variations of steam to carbon ratio

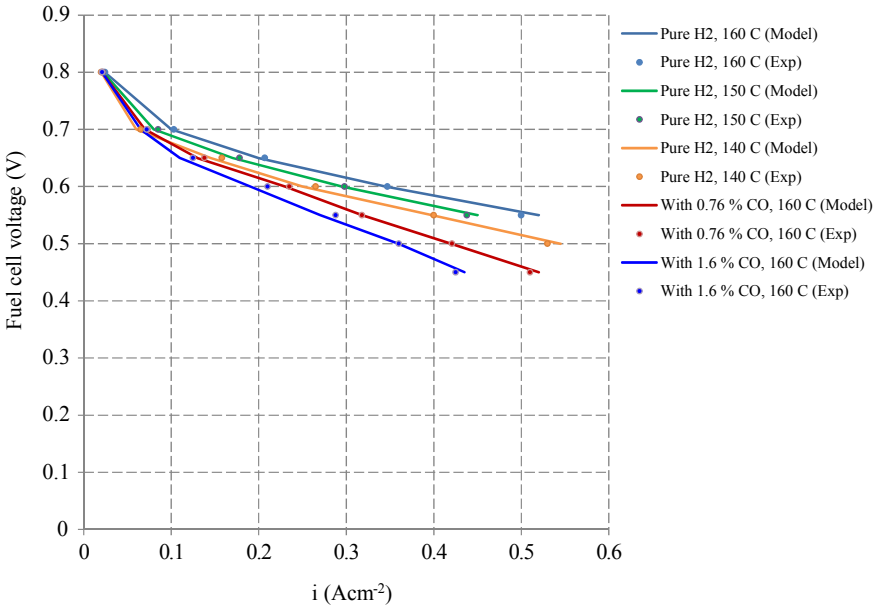

Fig. 3 – Validation of the developed model for the HT-PEM fuel cell stack.

and auxiliary to process fuel ratio on the performance of the system is first studied. In order to have a proper index for measuring the performance of the fuel processor, the reforming factor has been defined as follows:

$$RF = \frac{(\dot{m}_{H_2})_{anode-in} LHV_{H_2}}{(\dot{m}_{CH_4})_{tot} LHV_{CH_4}} \quad (28)$$

where $(\dot{m}_{H_2})_{anode-in}$ is the mass flow rate of hydrogen in the anodic inlet while $(\dot{m}_{CH_4})_{tot}$ is the total mass flow rate of methane which is consumed.

Based on the mentioned definition, four operating points, referring to combinations of these two parameters, with higher reforming factors and with wide range of CO molar fractions at the stack inlet have been chosen. Finally, for each of the chosen operating point, the effect of stack design parameters, including the temperature of the stack, the current density and the anodic stoichiometric ratio, on the performance of the system have been studied and discussed.

Fuel processor operating parameters

As the first investigation, the effect of variation in steam to carbon (S/C) ratio and auxiliary to process fuel flow rates (aux/proc) ratio on the performance of the system is studied. As demonstrated in Fig. 4, the investigation has been carried out for different aux/proc ratios (0.12–0.22) and a relatively wide range of S/C ratios (3.5–6).

As can be observed in Fig. 4, increasing the steam to carbon ratio results in enhancing the reforming factor up to a maximum and then a gradual decrement in this index. The mentioned behaviour of the reforming factor is attributed to the trade-off between the two competing effects of variations in steam to carbon ratio: First, an increment in S/C ratio leads to a higher rate of steam reforming reaction and consequently higher hydrogen production. On the other hand, increasing the S/C ratio requires higher flow rate of steam to be produced in the superheater which in turn results in lower temperature of the generated steam entering the SMR and consequently a decrement in the corresponding hydrogen conversion. Accordingly, the dominance of the first effect over the second one leads to an ascending trend in the reforming factor reaching an optimum at a specific S/C ratio, while the second effect becomes dominant after the optimum value and leads to the observed reduction in the reforming factor.

It can also be noticed that by escalating the aux/proc ratio, the maximum reforming factor is attained at greater S/C ratios. The stated behaviour corresponds to the point that utilizing higher auxiliary fuel provides higher heat to be supplied for generating steam hence the highest reforming factor can be gained at higher S/C ratios.

Boosting the S/C ratio, aside from the mentioned effect on the steam methane reforming reactions, can also enhance the rate of water gas shift reaction taking place in the reformer. As can be noticed in the mathematical model provided for the SMR, augmenting the rate of the steam reforming reaction enhances the carbon monoxide generation; while increasing the WGS reaction, which consumes CO, leads to a decrement in this component. However, as can be observed in Fig. 5, the corresponding effect of S/C on the WGS reaction is more

Table 5 – The operating parameters of the HT-PEMFC and LT-PEMFC based CHP plants.

Operative condition	HT-PEM based plant	LT-PEM based plant
Steam to carbon ratio (S/C)	4.5	4.5
Auxiliary to process flow rate ratio	0.12	0.175
Anodic stoichiometric ratio	1.2	1.6
Cathodic stoichiometric ratio	2	2
Current density (A cm^{-2})	0.2	0.2
Combustor outlet temperature (°C)	920	920
Cell temperature (°C)	160	66

Table 6 – Comparison of the performance indexes of HT-PEM based and LT-PEM based plant.

Performance index	HT-PEM based plant	LT-PEM based plant
Generated net electrical power (kW)	27.52	20.45
Generated total thermal power (kW)	49.87	53.24
Electrical efficiency (%)	29.21	21.18
Thermal efficiency (%)	52.93	55.13
First law efficiency (%)	82.15	76.31
PES (%)	17.50	6.07

dominant and the carbon monoxide molar fraction continuously decreases while boosting the S/C ratio. It can also be witnessed that increasing the aux/proc ratio increases the SMR reaction which in turn increases the CO concentration.

It is noteworthy that through the preceding analysis, in order to decouple the behaviour of the fuel processor and the stack, the stack current and the stack surface are chosen in a way that the current density and the anodic stoichiometric ratios would be kept constant.

As was previously pointed out in the HT-PEM fuel cell model, the operating conditions resulting in lower CO molar fractions will subsequently lead to higher cell voltages. Considering the fact that the gross electrical efficiency is in direct relation with both the reforming factor and the cell voltage, the gross electrical efficiency, as demonstrated in Fig. 6, does not necessarily have the same behaviour as the reforming factor since the cell voltage also has an effect. For instance, the obtained reforming factor for the operating conditions of aux/proc = 0.22 and S/C = 5.25 is more than the one obtained for aux/proc = 0.20 and S/C = 5.25, however as the first operating condition results in higher CO concentration and consequently lower cell voltage, the obtained gross electrical efficiency is less than one of the second operating point.

In order to conduct further investigations on the behaviour of the system, four operating conditions which result in higher reforming factors and electrical efficiencies and cover sufficiently wide range of CO concentration have been chosen. Table 7 includes the operating conditions of the selected cases and the obtained performance indices.

Stack design parameters

Cell temperature. As the first design parameter of the fuel cell stack, the effect of variations in the cell operating temperature on the performance of the system has been studied. As can be noticed in Fig. 7, increasing the cell operating temperature, for all of the considered cases, noticeably increases the cell voltage. The stated behaviour is related to the fact that increasing the operating temperature remarkably reduces the voltage losses and a subsequent significant increment in the cell voltage is witnessed. Considering the data given in Table 7, operating the system at different operating conditions (cases A to D) results in different carbon monoxide molar fraction at the stack inlet where the Case A results in the highest CO molar fraction (0.0063) and the Case D leads to the lowest one (0.0048). As a result, at each specific temperature, case D results in the highest achieved cell voltage which case A results in the lowest one. It can also be noted that by escalating the operating temperature, the difference between the cell voltages obtained for different cases is diminished and at the maximum temperature the achieved cell voltages are almost identical. This observed behaviour is attributed to the fact that at higher temperatures, carbon monoxide content will have less effect on the cell voltage. Fig. 8 shows the variations of the gross electrical efficiency with the stack operating temperature. Considering the fact that the generated power of the stack is the product of the number of cells, cell voltage and the current of the stack, the variation in the gross electrical efficiency is proportional to the product of the variations in the reforming factor and the cell voltage. As a result, for each specific case, the gross electrical efficiency increases with the temperature as the cell voltage is increasing while the reforming factor is kept almost constant. In a similar manner, at 160 °C, operating at case A results in higher reforming factor than the other cases while it leads to a lower

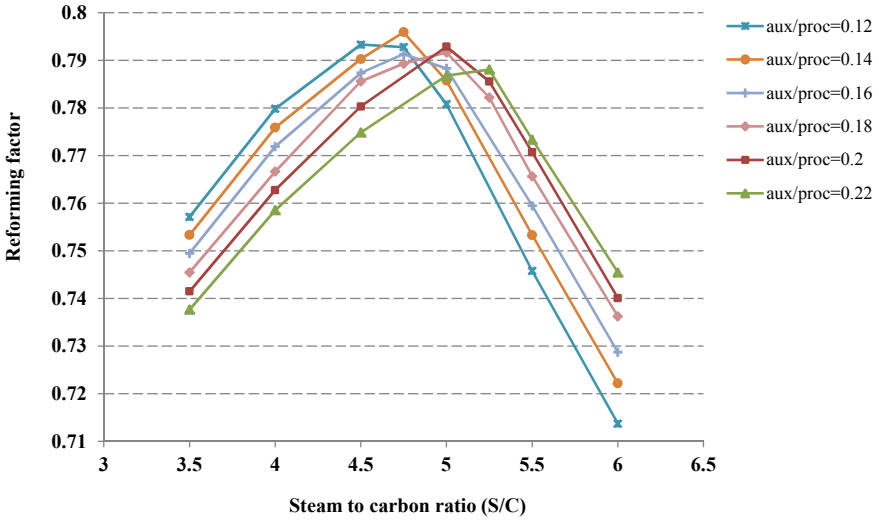

Fig. 4 – The effect of the aux/proc and S/C ratios on the reforming factor.

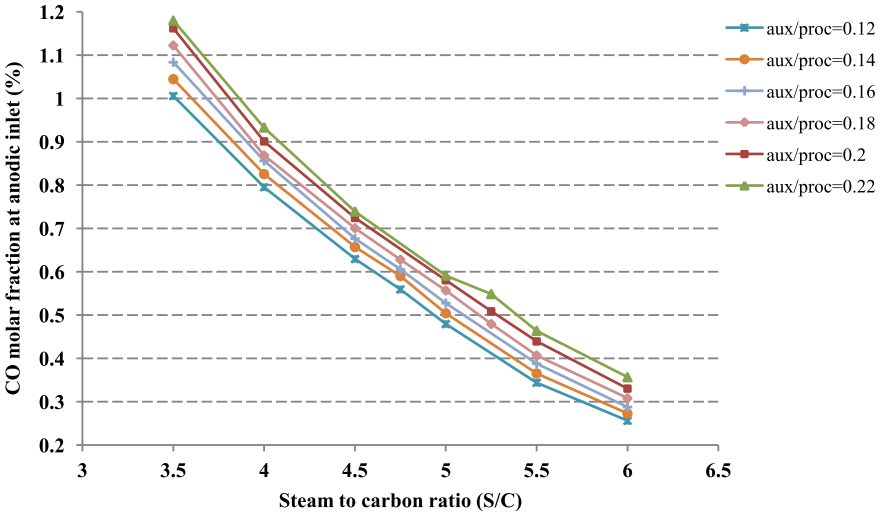

Fig. 5 – The effect of the aux/proc and S/C ratios on the CO molar fraction at anodic inlet.

cell voltage. However, the product of these two parameters will still be higher in case A than other cases and the corresponding achieved gross electrical efficiency will consequently be greater than the other ones. As the operating temperature increases, the difference between the obtained cell voltages decreases and accordingly this parameter cannot compensate the difference between the reforming factors and accordingly at higher operating temperatures, the difference between the achieved gross electrical efficiencies increases.

It is noteworthy that, although increasing the cell operating temperature significantly increases the obtained gross electrical efficiency, it inevitably augments the degradation of the stack. As presented in the previous study of the co-authors [44] increasing the operating temperature of the cell from 160 °C to 180 °C, at operating conditions similar to the ones considered in the present paper, results in rising the degra-dation rate from 8 μV h^{-1} to 19 μV h^{-1}. Hence, operating at elevated temperature, despite resulting in higher initial elec-trical efficiencies, can bring about lower overall long term performance of the system. Accordingly, determining the effective electrical efficiency of the plant through its lifetime, considering the degradation effects, can be a subject of further investigation.

Current density. Fig. 9 represents the impact of current density variation on the gross electrical efficiency for case A at different temperatures. As it can be noticed, there is a steady decrement in the efficiency while increasing the current density in all considered cell temperatures. For instance, for the operating temperature of 160 °C, the gross electrical efficiency experiences a continuous decline from 32.8% to 26.2% as the current density of the fuel cell is increased from 2000 to 4000 A m^{-2}. The observed considerable reduction in the fuel cell electrical efficiency is attributed to the fact that the fuel cell irreversibilities increase sharply with current density growth, which subsequently imposes a significant drop in the fuel cell voltage and power output of the stack. Despite the above mentioned detrimental effect of the increment in the

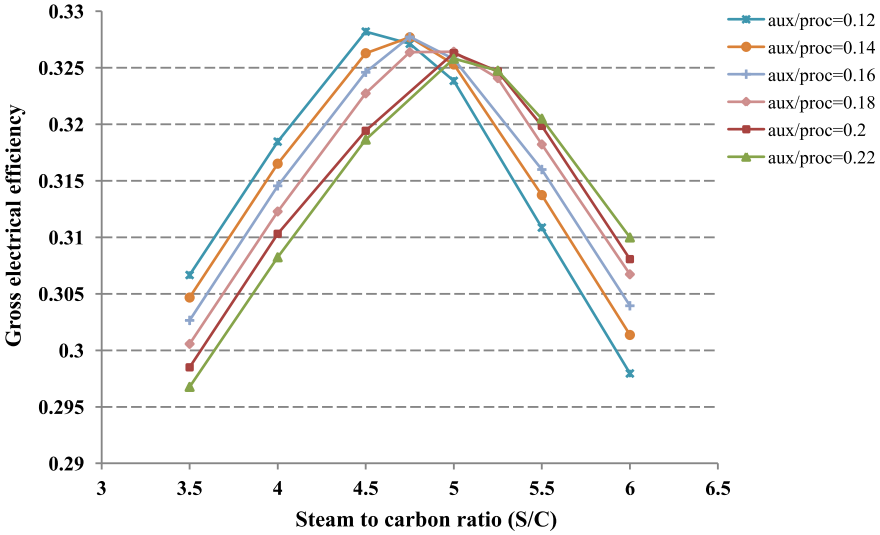

Fig. 6 – The effect of the S/C and aux/proc ratios on gross electrical efficiency.

Table 7 – Operating conditions of the chosen cases and their corresponding performance indexes.

Parameters	Case A	Case B	Case C	Case D
S/C ratio	4.50	4.75	5.00	5.25
Aux/proc ratio	0.12	0.14	0.16	0.18
Reforming factor (%)	79.33	79.59	78.83	78.21
CO concentration (%)	0.63	0.59	0.53	0.48
Stack power generation (kW)	30.92	31.42	31.79	31.17
Net electrical efficiency (%)	29.22	29.22	29.10	28.95

current density on the efficiency, one may consider the fact that an increase in the current density directly decreases the required active area of the fuel cell. In this regard, for the case of 160 °C, it can be determined that increasing the current from 2000 to 4000 A m^{-2} leads to a substantial reduction in the area of the cell from 564.8 to 283 m^2. Accordingly, the performed analysis shows a trade-off between electrical efficiency of the plant and an indicator of the required capital cost for the fuel cell stack and the optimum design point can be chosen based on the available investment and the desired efficiency of the plant.

As it was also discussed in the previous section, at any specific current density, operating at higher temperature results in a higher gross electrical efficiency. It can also be noted that any specific gross electrical efficiency can be obtained at higher current density while operating at higher temperatures. As an instance, operating at the current density of 2500 A m^{-2} and cell temperature of 160 °C results in almost the same gross electrical efficiency as operating at the current density of 4000 A m^{-2} and cell temperature of 180 °C. The mentioned trade-off between the cost of the stack and its corresponding durability, gives the designer the ability to employ a stack with lower surface, while keeping the efficiency at the desired level, by operating at higher temperatures, keeping in mind that this will decrease lifetime of the stack and consequently reduces the long-term performance of the plant.

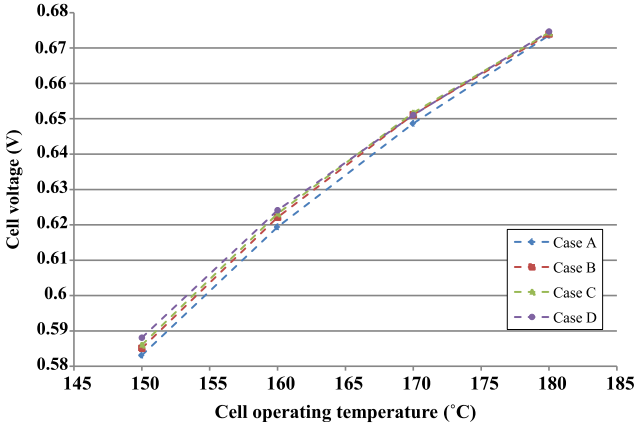

Fig. 7 – The effect of the cell operating temperature on the cell voltage; Case A: S/C = 4.50, Aux/proc = 0.12; Case B: S/C = 4.75, Aux/proc = 0.14; Case C: S/C = 5.00, Aux/proc = 0.16; Case D: S/C = 5.25, Aux/proc = 0.18 (other operating parameters for all of the cases are chosen to be the same as the ones given in Table 5).

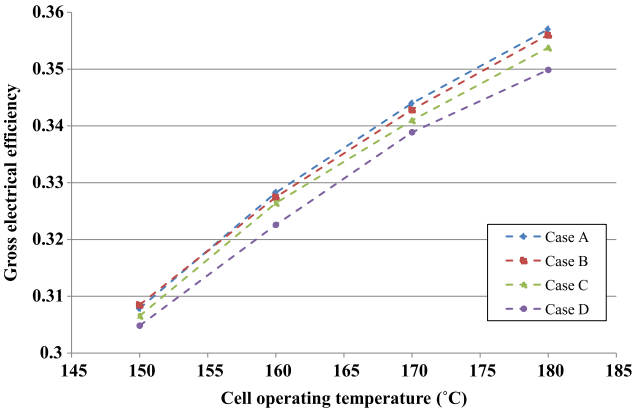

Fig. 8 – The variations of the gross electrical efficiency with the cell operating temperature.

Anodic stoichiometric ratio. The present section is devoted to the investigation of the effect of the changes in the anodic stoichiometric ratio (λ_{H_2}) on the performance of the plant. In order to investigate the effect of this parameter and to decouple the corresponding impact from other variables, the imposed total current of the plant should be changed, while the area of the stack is varied in order to keep the current density constant. A descending profile of gross electrical efficiency versus anodic stoichiometric ratio for all the cases can be observed in Fig. 10. The main reason of this behaviour is due to the fact that increasing the λ_{H_2} decreases the amount of exploited hydrogen within the stack which adversely affects the electrical power output of the stack and the efficiency. On the other hand, by increasing the anodic stoichiometric ratio, the amount of unconsumed hydrogen at the anodic outlet, which is next injected into the burner, rises. As a result, the available amount of heat of the combustion gases leaving the burner enhances and subsequently more thermal power, both to the SMR and the economizer, is supplied. Owing to the increase in the economizer's thermal generation, there is an upward trend in the thermal efficiency of the CHP plant from 53% to 55.5% due to an increment (from 1.2 to 1.6) in the anodic stoichiometric ratio.

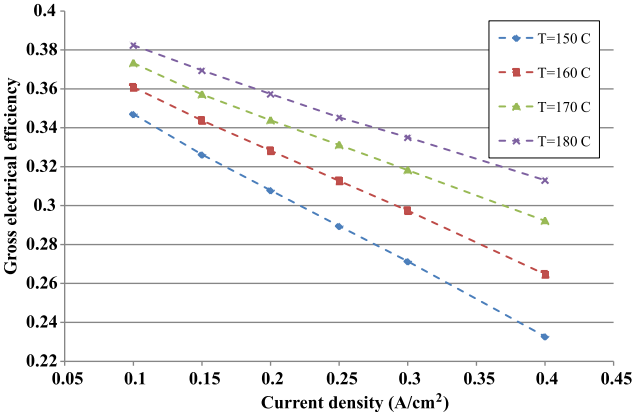

Fig. 9 – The effect of current density on the gross electrical efficiency while operating at four different cell temperature (Fuel processor design parameters are chosen according to the design parameters of Case A).

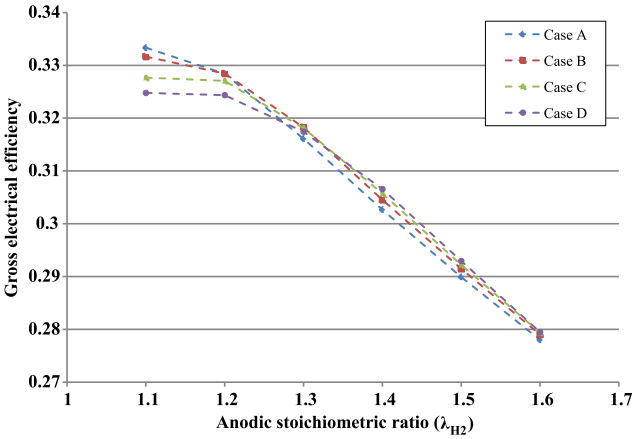

Fig. 10 – The effect of variations of anodic stoichiometric ratio on the gross electrical efficiency.

The effect of the increment in the heat provided by the combustion gases to the SMR can be observed in the variation of CO molar fractions. Fig. 11 depicts the profile of CO molar fractions at the inlet of the anode versus anodic stoichiometric ratio of the stack. An ascending trend can be vividly noticed in all cases which strongly justifies the favourable effect of higher available heat (at higher anodic stoichiometric ratios) in the combustion gas side on the kinetic of the first reforming reaction in which CO is produced. It worth noting that a significant difference of CO molar fractions can be observed in lower λ_{H_2} compared to the negligible difference at higher anodic stoichiometric ratios. The mentioned behaviour is attributed to the fact that by increasing the S/C ratio (from case A to D), higher flow rate of steam should be produced in the superheater, hence at low λ_{H_2} sufficient heat is not available to be supplied to the superheater and consequently the outlet steam temperature decreases; while at higher λ_{H_2} the available heat at the superheater is augmented and the decrement in the outlet temperature of the steam is significantly suppressed. The reduction in the steam outlet temperature and subsequently the temperature of the SMR feed reduces the rate of first steam reforming reaction and CO

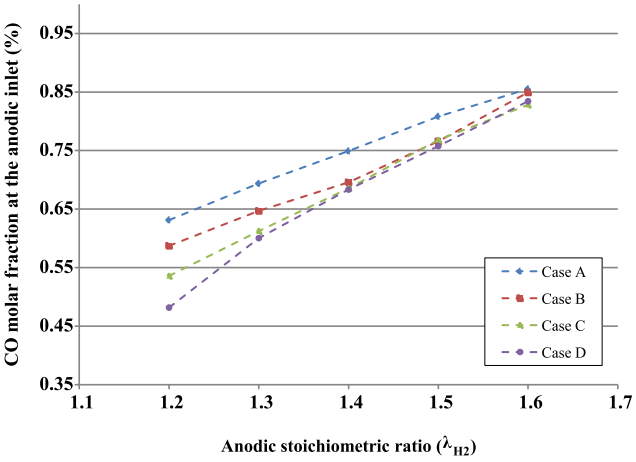

Fig. 11 – Effect of variations of anodic stoichiometric ratio on CO molar fraction at stack inlet.

concentration at the outlet; the effect which can be observed in the notable difference between the CO concentrations obtained for different cases at $\lambda_{H_2} = 1.2$.

It is worth mentioning that the average molar fraction of the carbon monoxide within the channel determines the negative effect of CO on the cell voltage. Hence, despite the fact that the CO molar fractions at low anodic stoichiometric ratios are less than their corresponding value at larger ones, since more hydrogen is utilized at lower λ_{H_2}, inferior cell voltage might be achieved. As an example for Case A, the cell voltage at $\lambda_{H_2} = 1.2$ is 0.619 V while it is boosted up to 0.623 V at $\lambda_{H_2} = 1.6$ due to the mentioned effect.

Conclusion

In the present study, a new configuration for an existing LT-PEM fuel cell based micro CHP plant (Sidera30) was proposed. In the new system, the conventional LT-PEM stack is replaced with an HT-PEM one and it was demonstrated that due to the advantages of this type of PEM fuel cells, the obtained electrical efficiency of the previous system (21.2%) can be increased up to 29.2%. In the second part of the work, a parametric study on the fuel processor design parameters was first conducted and four pairs of fuel auxiliary to process ratio and steam to carbon ratio, leading to the highest gross electrical efficiencies, were selected. In the next step, for each chosen case, the effects of stack design parameters including the cell operating temperature, the current density and the anodic stoichiometric ratio on the overall performance of the micro CHP plant were studied. It was demonstrated that increasing the cell operating temperature (from 160 to 180 °C) can improve the gross electrical efficiency from 30.7% to 35.8%. It was also shown that operating at higher temperature significantly decreases the effect of CO concentration on the cell voltage and subsequent electrical efficiency. Furthermore, increasing the anodic stoichiometric ratio from 1.2 to 1.6 lowers the gross electrical efficiency from 32.8% to 27.9% while it leads to an enhancement of the thermal generation from 48.6 kW to 52.6 kW which clearly assures the capability of the system to be adjusted to the variations in the thermal and electrical demands. Finally, it was elaborated that by doubling the current density of the fuel cell, a 50% decrement in the required active area of the stack would be acquired even though it results in a 6.8% reduction in the gross electrical efficiency.

Acknowledgement

The authors would like to acknowledge ICI Caldaie S.p.A for providing technical and financial support for this project. The employed data has been extracted from the results of Real-FC project funded by Lombardy Region.

REFERENCES

[1] Zhang J, Xie Z, Zhang J, Tang Y, Song C, Navessin T, et al. High temperature PEM fuel cells. J Power Sources 2006;160:872–91.

[2] Mehta V, Cooper JS. Review and analysis of PEM fuel cell design and manufacturing. J Power Sources 2003;114:32–53.
[3] Sone Y, Ueno M, Kuwajima S. Fuel cell development for space applications: fuel cell system in a closed environment. J Power Sources 2004;137:269–76.
[4] Rinaldi F, Marchesi R. Polimeric electrolyte membrane fuel cells: characterization test under variable temperature and relative humidity conditions. J Fuel Cell Sci Tech 2006;4:231–7.
[5] Romero-Pascual E, Soler J. Modelling of an HTPEM-based micro-combined heat and power fuel cell system with methanol. Int J Hydrogen Energy 2014;39:4053–9.
[6] Nagata Y. Quantitative analysis of CO_2 emissions reductions through introduction of stationary-type PEM-FC systems in Japan. Energy 2005;30:2636–53.
[7] Obara Sy, Tanno I. Study on capacity optimization of PEM fuel cell and hydrogen mixing gas-engine compound generator. Int J Hydrogen Energy 2007;32:4329–39.
[8] Hwang JJ, Zou ML. Development of a proton exchange membrane fuel cell cogeneration system. J Power Sources 2010;195:2579–85.
[9] Shabani B, Andrews J. An experimental investigation of a PEM fuel cell to supply both heat and power in a solar-hydrogen RAPS system. Int J Hydrogen Energy 2011;36:5442–52.
[10] Ferguson A, Ismet Ugursal V. Fuel cell modelling for building cogeneration applications. J Power Sources 2004;137:30–42.
[11] Radulescu M, Lottin O, Feidt M, Lombard C, Le Noc D, Le Doze S. Experimental and theoretical analysis of the operation of a natural gas cogeneration system using a polymer exchange membrane fuel cell. Chem Eng Sci 2006;61:743–52.
[12] Calise F, Ferruzzi G, Vanoli L. Transient simulation of polygeneration systems based on PEM fuel cells and solar heating and cooling technologies. Energy 2012;41:18–30.
[13] Hubert C-E, Achard P, Metkemeijer R. Study of a small heat and power PEM fuel cell system generator. J Power Sources 2006;156:64–70.
[14] Najafi B, Shirazi A, Aminyavari M, Rinaldi F, Taylor RA. Exergetic, economic and environmental analyses and multi-objective optimization of an SOFC-gas turbine hybrid cycle coupled with an MSF desalination system. Desalination 2014;334:46–59.
[15] Shirazi A, Najafi B, Aminyavari M, Rinaldi F, Taylor RA. Thermal–economic–environmental analysis and multi-objective optimization of an ice thermal energy storage system for gas turbine cycle inlet air cooling. Energy 2014;69:212–26.
[16] Shabani B, Andrews J, Watkins S. Energy and cost analysis of a solar-hydrogen combined heat and power system for remote power supply using a computer simulation. Sol Energy 2010;84:144–55.
[17] Staffell I, Green R. The cost of domestic fuel cell micro-CHP systems. Int J Hydrogen Energy 2013;38:1088–102.
[18] Contreras A, Posso F, Guervos E. Modelling and simulation of the utilization of a PEM fuel cell in the rural sector of Venezuela. Appl Energy 2010;87:1376–85.
[19] Guizzi GL, Manno M. Fuel cell-based cogeneration system covering data centers' energy needs. Energy 2012;41:56–64.
[20] Roses L, Manzolini G, Campanari S. CFD simulation of Pd-based membrane reformer when thermally coupled within a fuel cell micro-CHP system. Int J Hydrogen Energy 2010;35:12668–79.
[21] Subianto S, Pica M, Casciola M, Cojocaru P, Merlo L, Hards G, et al. Physical and chemical modification routes leading to improved mechanical properties of perfluorosulfonic acid membranes for PEM fuel cells. J Power Sources 2013;233:216–30.
[22] Jeon Y, Hwang H-k, Park J, Hwang H, Shul Y-G. Temperature-dependent performance of the polymer electrolyte membrane fuel cell using short-side-chain perfluorosulfonic acid ionomer. Int J Hydrogen Energy.
[23] Cheddie D, Munroe N. Mathematical model of a PEMFC using a PBI membrane. Energy Convers Manag 2006;47:1490–504.
[24] Li Q, He R, Jensen JO, Bjerrum NJ. PBI-based polymer membranes for high temperature fuel cells – Preparation, characterization and fuel cell demonstration. Fuel Cells 2004;4:147–59.
[25] Baschuk JJ, Li X. Carbon monoxide poisoning of proton exchange membrane fuel cells. Int J Energy Res 2001;25:695–713. 2001;25.
[26] Baschuk JJ, Li X. Modelling CO poisoning and O2 bleeding in a PEM fuel cell anode. Int J Energ Res 2003;27:1095–116. 2001;25.
[27] Korsgaard AR, Nielsen MP, Kær SK. Part one: a novel model of HTPEM-based micro-combined heat and power fuel cell system. Int J Hydrogen Energy 2008;33:1909–20.
[28] Mocotéguy P, Ludwig B, Scholta J, Nedellec Y, Jones DJ, Rozière J. Long-term testing in dynamic mode of HT-PEMFC H_3PO_4/PBI celtec-P based membrane electrode assemblies for micro-CHP applications. Fuel Cells 2010;10:299–311.
[29] Korsgaard AR, Refshauge R, Nielsen MP, Bang M, Kær SK. Experimental characterization and modeling of commercial polybenzimidazole-based MEA performance. J Power Sources 2006;162:239–45.
[30] Oono Y, Sounai A, Hori M. Influence of the phosphoric acid-doping level in a polybenzimidazole membrane on the cell performance of high-temperature proton exchange membrane fuel cells. J Power Sources 2009;189:943–9.
[31] Zhang J, Tang Y, Song C, Zhang J. Polybenzimidazole-membrane-based PEM fuel cell in the temperature range of 120–200°C. J Power Sources 2007;172:163–71.
[32] Arsalis A, Nielsen MP, Kær SK. Modeling and parametric study of a 1 kWe HT-PEMFC-based residential micro-CHP system. Int J Hydrogen Energy 2011;36:5010–20.
[33] Arsalis A, Nielsen MP, Kær SK. Modeling and optimization of a 1 kWe HT-PEMFC-based micro-CHP residential system. Int J Hydrogen Energy 2012;37:2470–81.
[34] Jannelli E, Minutillo M, Perna A. Analyzing microcogeneration systems based on LT-PEMFC and HT-PEMFC by energy balances. Appl Energy 2013;108:82–91.
[35] Adris AM, Pruden BB, Lim CJ, Grace JR. On the reported attempts to radically improve the performance of the steam methane reforming reactor. Can J Chem Eng 1996;74:177–86.
[36] Xu J, Froment GF. Methane steam reforming, methanation and water–gas shift: I. Intrinsic kinetics. AIChE J 1989;35:88–96.
[37] Posada A, Manousiouthakis V. Heat and power integration of methane reforming based hydrogen production†. Ind Eng Chem Res 2005;44:9113–9.
[38] Keiski RL, Salmi T, Niemistö P, Ainassaari J, Pohjola VJ. Stationary and transient kinetics of the high temperature water-gas shift reaction. Appl Catal A General 1996;137:349–70.
[39] Siegel C, Bandlamudi G, Heinzel A. Systematic characterization of a PBI/H_3PO_4 sol–gel membrane—modeling and simulation. J Power Sources 2011;196:2735–49.
[40] Pisani L. Multi-component gas mixture diffusion through porous media: a 1D analytical solution. Int J Heat Mass Transf 2008;51:650–60.
[41] Poling BE, Prausnitz JM, O'Connell JP. The properties of gases and liquids. McGraw-Hill; 2001.
[42] Liu Z, Wainright JS, Litt MH, Savinell RF. Study of the oxygen reduction reaction (ORR) at Pt interfaced with phosphoric acid doped polybenzimidazole at elevated temperature and low relative humidity. Electrochim Acta 2006;51:3914–23.

[43] Bergmann A, Gerteisen D, Kurz T. Modelling of CO poisoning and its dynamics in HTPEM fuel cells. Fuel Cells 2010;10:278–87.
[44] Galbiati S, Baricci A, Casalegno A, Marchesi R. Degradation in phosphoric acid doped polymer fuel cells: a 6000 h parametric investigation. Int J Hydrogen Energy 2013;38:6469–80.
[45] He S, Li Y, Wang RZ. Progress of mathematical modeling on ejectors. Renew Sustain Energy Rev 2009;13:1760–80.
[46] Fundamentals of heat and mass transfer. 6th ed. Wiley India Pvt Limited; 2010.
[47] Churchill SW, Bernstein M. A correlating equation for forced convection from gases and liquids to a circular cylinder in crossflow. J Heat Transf 1977;99:300–6.
[48] Campanari S, Valenti G, Macchi E, Lozza G, Ravidà N. Development of a micro-cogeneration laboratory and testing of a natural gas CHP unit based on PEM fuel cells. Appl Therm Eng.